Unified Statistical Performance of FSO Link due to the Combined Effect of Weak Turbulence and Generalized Pointing Error with HD and IM/DD

Kug-Jin Jung, Sung Sik Nam, Jinwoo Shin, and Young-Chai Ko

Abstract: **In this paper, we set up the statistical channel model of ship-to-ship (or ship-to-shore) free space optical links considering generalized pointing error and weak turbulence. We combine various pointing error models with weak turbulence and derive the composite probability density functions (PDF) for each case of pointing error model. Also, using the similarity of the composite PDFs, we obtain a unified expression for the composite PDF. Furthermore, we conduct error rate analysis based on both intensity modulation and direct detection (IM/DD) and heterodyne detection (HD). At last, the numerical results confirm that the derived average error rate gives precise prediction on error rate.**

Index Terms: **Free space optical communication, heterodyne detection, IM/DD, pointing error, weak turbulence.**

I. INTRODUCTION

FREE -space optical communication (FSO) has been proposed as an attractive alternative to radio frequency communication in the sense that it provides wide bandwidth and high capacity without requirement of license. However, the scalability of FSO link is limited by pointing error, atmospheric turbulence, and loss [2]. Especially, when it comes to the FSO link between moving platforms, it is imperative works to analyze the statistical channel model considering accurate pointing errors and atmospheric turbulence at the same time [3].

The pointing error represents the displacement between the laser beam and the aperture of detector, and it can be analyzed by the horizontal and vertical displacements where both follow Gaussian distributions. Pointing error is composed of boresight and jitter. The boresight is the fixed displacement between each center while the jitter is random offset [4].

The performance analysis of pointing error combined with weak turbulence has been studied in [4]–[10]. Authors in [5] derived composite channel model considering pointing error and turbulence and optimized the beamwidth to maximize the capacity. A unified capacity expression that accounts for intensity modulation and direct detection (IM/DD) and heterodyne detection (HD) under the weak turbulence was derived in [6]. In [7]–[9], bit error rate (BER) and outage probability were investigated under weak turbulence with the effect of pointing error using M-ary amplitude shift keying modulation, subcarrier intensity modulation differential phase shift keying (SIM-DPSK), and direct current biased optical orthogonal frequency division multiplexing (DCO-OFDM) respectively. However, the research groups in [6]–[9] assumed that the pointing error model follows Rayleigh distribution and utilized the composite probability density function (PDF) derived in [5]. Accordingly, the results represent only one specific pointing error model and the channel model is not suitable for describing various types of pointing errors described in [11]. In [4], authors derived composite PDF considering more general pointing error model with nonzero boresight and conducted performance analysis. Also, authors in [10] considered the nonzero boresight pointing error with Malaga modeled turbulence which is suitable for weak to strong turbulence conditions and derived the average BER expression for IM/DD FSO link. Nevertheless, the derivation of composite PDF for log-normal turbulence is ambiguous and the results in [4], [10] are limited to one pointing error model with IM/DD.

To the best of our knowledge, no studies have considered various types of pointing error model with weak turbulence. Accordingly, the BER analysis of both IM/DD and HD based on various pointing error models under weak turbulence has not been conducted. For the strong turbulence as Gamma Gamma fading, the statistical analysis with various pointing error models was dealt in [12]. In this paper, FSO links between ships or between shore and ship are considered and the effects of typical ship movements are analyzed. Then, by applying it to the pointing error models described in [11], we derive unified composite PDF results combining pointing error and weak atmospheric turbulence. Utilizing the unified composite PDF, we investigate the BER performance of FSO system based on both IM/DD and HD.

The rest of this paper is organized as follows. Section II presents a statistical model for weak atmospheric turbulence and introduces various pointing error models of moving platforms suggested in [11]. In Section III, we statistically obtain the composite PDF results for the pointing error models based on the weak turbulence model, and then with these results, we derive them as the unified composite PDF expression. Then, with the unified composite PDF result, we analyze the BER performance

This is an extended version of paper which was presented in CSCN (2019) [1].
Manuscript received October 17 2020; approved for publication October 26, 2020. This paper is specially handled by EIC and Division Editor with the help of three anonymous reviewers in a fast manner.
This work was supported by a grant to Terahertz Electronic Device Research Laboratory funded by Defense Acquisition Program Administration, and by Agency for Defense Development(UD180025RD).
K. -J. Jung and Y. -C. Ko are with the School of Electrical Engineering, Korea University, Seoul, South Korea, email: {kug0860, koyc}@korea.ac.kr.
S. S. Nam is with the Electronic Engineering, Gachon University, South Korea, email: ssnam@gachon.ac.kr.
J. Shin is with the Agency for Defense Development, Daejeon, South Korea, email: sjinu@add.re.kr.
Y. -C. Ko and S. S. Nam are the corresponding authors.
Digital Object Identifier: 10.23919/JCN.2020.000030

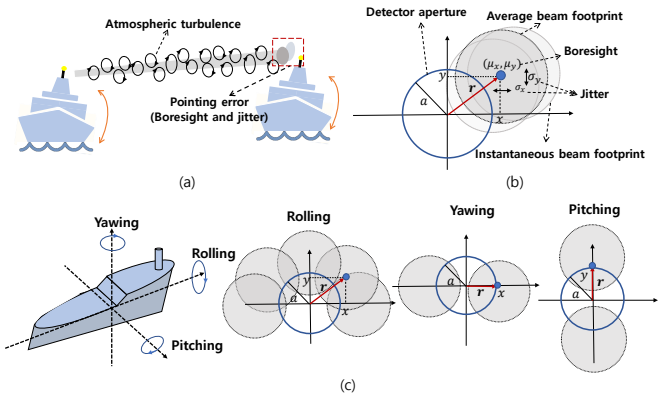

Fig. 1. Channel Modeling in FSO between ships: (a) Communication between ships, (b) pointing error, and (c) pointing error models between ships.

in FSO communication based on IM/DD and HD in Section IV. In Section V, we describe the simulation setup and then cross-verify these analytical results with the Monte-Carlo simulation results under various pointing error models and weak turbulence conditions. Finally, we conclude our paper in Section VI.

II. SYSTEM AND CHANNEL MODEL

Assuming that the transmitted signal x is distorted by channel gain h, and additive white Gaussian noise (AWGN) n with variance N_0, we can express the received signal y as

$$y = \eta_e h x + n, \tag{1}$$

where η_e is the effective photo-electric conversion ratio. In a typical FSO link, the channel gain h can be modeled as $h = h_l h_a h_p$, where h_l is the atmospheric loss factor, h_a is the atmospheric fading factor, and h_p is the pointing error factor. Note that h_l is deterministic and both h_a and h_p are random variables (RV). h_l can be given as $h_l = \exp(-\sigma z)$ where σ is attenuation coefficient and z is link distance [13]. The statistical characteristic of random variables h_a and h_p is presented below, respectively.

A. Atmospheric Turbulence

As we assume that a signal is transmitted by a plane wave in weak turbulence conditions, h_a can be statistically modeled by lognormal fading. The PDF of h_a is given by [14]

$$f_{h_a}(h_a) = \frac{1}{2h_a\sqrt{2\pi\sigma_X^2}} \exp\left(-\frac{\left(\ln h_a + 2\sigma_X^2\right)^2}{8\sigma_X^2}\right), \tag{2}$$

where σ_X^2 represents the log-amplitude variance and is approximately expressed by Rytov variance, σ_R^2 as $\sigma_X^2 \approx \sigma_R^2/4$. The Rytov variance is defined as $\sigma_R^2 = 1.23k^{7/6}C_n^2 z^{11/6}$ where k, z, and C_n^2 represent the optical wavenumber, the propagation distance, and the refractive index structure parameter, respectively [14]. The nth moment of h_a is given by [11]

$$\mathbb{E}\left[h_p^n\right] = \exp\left(2n\sigma_X^2(n-1)\right). \tag{3}$$

B. Pointing Error

Fig. 1(a) depicts main channel factors in FSO communication which are atmospheric turbulence and pointing error. Especially for the pointing error, there are two main movement factor as shown in Fig. 1(b), jitter and boresight, where the jitter is random offset of the beam center while the boresight is a fixed displacement between a detector aperture and an average beam footprint [4]. Movement of ships can be classified into rolling, yawing, and pitching as shown in Fig. 1(c) and the movements can lead to modeling the pointing error in FSO communication between ships or between shore and ship as follows. As yawing and pitching leads to displacement in only x or y axis while rolling occurs in both x and y axes, rolling can be modeled by the double sided pointing error model while yawing and pitching can be modeled by the single-sided pointing error. Further, if the ship is affected by two or more of the three main factors, the pointing error can be modeled as a double-sided error [1].

Assuming a Gaussian beam with beamwidth w_z and detector with aperture radius of a, the fraction of the collected power can be approximated at the distance z as shown in [5]

$$h_p(r;z) \approx A_0 \exp\left(-\frac{2r^2}{w_{z_{eq}}^2}\right). \tag{4}$$

In (4), as shown in Fig. 1(b), r is the radial displacement between the beam and the centers of detector, $A_0 = [\mathrm{erf}(v)]^2$ is the fraction of collected power at $r = 0$ when the ratio between the beamwidth and the aperture radius is $v = \sqrt{(a^2\pi/2{w_z}^2)}$, and $w_{z_{eq}} = \sqrt{w_z^2 \frac{\sqrt{A_0\pi}}{2v\exp(-v^2)}}$ is the equivalent beamwidth, where $\mathrm{erf}(x) = \frac{2}{\sqrt{\pi}}\int_0^x e^{-t^2}dt$ is the error function. The approximation in (4) is valid when $w_z > 6a$ which can be obtained by typical FSO communication systems [5]. Further, the radial displacement vector in Fig. 1(b) can be written as $\mathbf{r} = [r_x, r_y]^T$ where r_x and r_y follow independent Gaussian distribution as $r_x \sim \mathcal{N}(\mu_x, \sigma_x^2)$, and $r_y \sim \mathcal{N}(\mu_y, \sigma_y^2)$, respectively. Then the radial displacement can be expressed as $r = |\mathbf{r}| = \sqrt{r_x^2 + r_y^2}$. According to its boresight and jitter, the pointing error models can be classified into 1) 'nonzero boresight and identical jitter' case, 2) 'zero boresight and non-identical jitter' case, and 3) 'nonzero boresight and single jitter' case as shown in [11]. In each case, the radial displacement r follows 1) Rician, 2) Hoyt, and 3) nonzero mean single sided Gaussian distribution, respectively and the corresponding PDF and nth momentum of h_p are listed in Table 1 and Table 2, respectively. Utilizing them, we derive composite PDF of each case of the pointing error model with the weak turbulence and unified expression in the next section.

III. STATISTICAL ANALYSIS OF COMPOSITE PDF

A. Special Cases

The statistical characteristics of channel gain $h = h_l h_a h_p$ can be assumed as [5]

$$f_h(h) = \int \frac{1}{h_a h_l} f_{h_p}\left(\frac{h}{h_a h_l}\right) f_{h_a}(h_a)\, dh_a. \tag{11}$$

Table 1. Distribution of h_p, $f_{h_p}(\cdot)$, $0 \le h_p \le A_0$ [11].

Rician
$$\frac{\varepsilon^2 \exp\left(\frac{-s^2}{2\sigma^2}\right)}{{A_0}^{\varepsilon^2}} {h_p}^{\varepsilon^2-1} I_0\left(\frac{s}{\sigma^2}\sqrt{\frac{w_{z_{eq}}^2 \ln\frac{A_0}{h_p}}{2}}\right) \quad (5)$$
Hoyt
$$\frac{\varepsilon_x \varepsilon_y}{A_0}\left(\frac{h_p}{A_0}\right)^{\frac{\varepsilon_x^2\left(1+l^2\right)}{2}-1} I_0\left(\frac{\varepsilon_x^2\left(l^2-1\right)}{2}\ln\frac{A_0}{h_p}\right) \quad (6)$$
Nonzero mean single sided
$$\frac{\varepsilon^2 {h_p}^{\varepsilon^2-1}}{{A_0}^{\varepsilon^2}}\sqrt{\frac{2\mu}{w_{z_{eq}}\sqrt{2\ln\frac{A_0}{h_p}}}}\exp\left(-\frac{2\mu^2\varepsilon^2}{w_{z_{eq}}^2}\right) \times I_{-\frac{1}{2}}\left(\frac{2\mu\varepsilon^2}{w_{z_{eq}}}\sqrt{2\ln\frac{A_0}{h_p}}\right) \quad (7)$$

Table 2. nth moment of h_p, $\mathbb{E}\left[h_p^n\right]$ [11].

Rician
$$\frac{A_0^n \varepsilon^2}{n+\varepsilon^2}\exp\left(-\frac{2n\varepsilon^2 s}{w_{z_{eq}}^2\left(n+\varepsilon^2\right)}\right) \quad (14)$$
Hoyt
$$\frac{A_0^n \varepsilon_x \varepsilon_y}{\sqrt{\left(\varepsilon_x^2+n\right)\left(\varepsilon_y^2+n\right)}} \quad (15)$$
Nonzero mean single sided
$$\frac{A_0^n \varepsilon}{\sqrt{n+\varepsilon^2}}\exp\left(-\frac{2n\mu^2\left(n+2\varepsilon^2\right)}{w_{z_{eq}}^2\left(n+\varepsilon^2\right)}\right) \quad (16)$$

A.1 Rician

We substitute (5) which is PDF of h_p in case of Rician model and (2) into (11). After some mathematical manipulation, the composite PDF under weak turbulence can be expressed as

$$\begin{aligned} f(h) =& \frac{\varepsilon^2 e^{-\frac{s^2}{2\sigma^2}} h^{\varepsilon^2-1}}{2(A_0 h_l)^{\varepsilon^2}\sqrt{2\pi\sigma_X^2}} \int_{\frac{h}{A_0 h_l}}^{\infty} {h_a}^{-\varepsilon^2-1} \\ & \times I_0\left(\frac{s}{\sigma^2}\sqrt{\frac{-w_{z_{eq}}^2 \ln\left(\frac{h}{A_0 h_l h_a}\right)}{2}}\right) \\ & \times \exp\left(-\frac{\left(\ln h_a + 2\sigma_X^2\right)^2}{8\sigma_X^2}\right) dh_a, \end{aligned} \quad (12)$$

where $I_\nu(\cdot)$ denotes the ν th-order modified Bessel function of the first kind [15, eq. (8.431.1)]. We replace the $I_0(\cdot)$ in (12) with series representation of [15, eq. (8.445)], and change the order of the integral and infinite summation with mathematical manipulation as

$$\begin{aligned} f(h) =& \frac{\varepsilon^2 e^{-\frac{s^2}{2\sigma^2}} h^{\varepsilon^2-1}}{2(A_0 h_l)^{\varepsilon^2}\sqrt{2\pi\sigma_X^2}} \sum_{k=0}^{\infty}\frac{1}{(k!)^2}\left(\frac{s^2 w_{z_{eq}}^2}{8\sigma^4}\right)^k \\ & \times \int_{\frac{h}{A_0 h_l}}^{\infty} {h_a}^{-\varepsilon^2-1}\left(\ln\frac{A_0 h_l h_a}{h}\right)^k \\ & \times \exp\left(-\frac{\left(\ln h_a + 2\sigma_X^2\right)^2}{8\sigma_X^2}\right) dh_a. \end{aligned} \quad (13)$$

By letting $y = \ln\left(A_0 h_l h_a / h\right)$, (13) can be written as the function of y as

$$\begin{aligned} f(h) =& \frac{\varepsilon^2 e^{-\frac{s^2}{2\sigma^2}} h^{\varepsilon^2-1}}{2(A_0 h_l)^{\varepsilon^2}\sqrt{2\pi\sigma_X^2}}\left(\frac{h}{A_0 h_l}\right)^{-\varepsilon^2-\frac{1}{2}} \\ & \times \exp\left(-\frac{\left(\ln\frac{h}{A_0 h_l}\right)^2}{8\sigma_X^2} - \frac{\sigma_X^2}{2}\right)\sum_{k=0}^{\infty}\frac{1}{(k!)^2}\left(\frac{s^2 w^2}{8\sigma^4}\right)^k \\ & \times \int_0^{\infty} y^k \exp\left(-\frac{y^2}{8\sigma_X^2} - \left(\frac{\ln\frac{h}{A_0 h_l}}{4\sigma_X^2} + \varepsilon^2 + \frac{1}{2}\right)y\right) dy. \end{aligned} \quad (17)$$

Then, with the help of an integral identity in [15, eq. (3.462.1)], the series representation of the composite PDF can be written as

$$\begin{aligned} f(h) =& \frac{\varepsilon^2 e^{-\frac{s^2}{2\sigma^2}} h^{\varepsilon^2-1}}{(A_0 h_l)^{\varepsilon^2}\sqrt{2\pi}} \exp\left(-\frac{A^2(h)}{4} + 2\sigma_X^2\varepsilon^2 + 2\sigma_X^2\varepsilon^4\right) \\ & \times \sum_{k=0}^{\infty}\frac{1}{k!}\left(\frac{s^2 w_{z_{eq}}^2 \sigma_X}{4\sigma^4}\right)^k D_{-k-1}\left(A(h)\right), \end{aligned} \quad (15)$$

where $A(h) = \frac{\ln\left(\frac{h}{A_0 h_l}\right) + 2\sigma_X^2 + 4\sigma_X^2\frac{\varepsilon_x^2+\varepsilon_y^2}{2}}{2\sigma_X}$ and $D(\cdot)$ is parabolic cylinder function [15, eq. (9.240)]. In this case, $\varepsilon_x = \varepsilon_y = \varepsilon$.

A.2 Hoyt

By substituting (6) and (2) into (11), the composite PDF of Hoyt pointing error model case can be expressed as

$$\begin{aligned} f(h) =& \frac{\varepsilon_x \varepsilon_y h^{\frac{\varepsilon_x^2+\varepsilon_y^2}{2}-1}}{2(A_0 h_l)^{\frac{\varepsilon_x^2+\varepsilon_y^2}{2}}\sqrt{2\pi\sigma_X^2}} \int_{\frac{h}{A_0 h_l}}^{\infty} {h_a}^{-\frac{\varepsilon_x^2+\varepsilon_y^2}{2}-1} \\ & \times I_0\left(\frac{\varepsilon_x^2-\varepsilon_y^2}{2}\ln\left(\frac{h}{A_0 h_l h_a}\right)\right) \\ & \times \exp\left(-\frac{\left(\ln h_a + 2\sigma_X^2\right)^2}{8\sigma_X^2}\right) dh_a. \end{aligned} \quad (16)$$

With similar procedure of replacing $I_0(\cdot)$ with series representation, swapping the integral and infinite summation, and change of variable, we can rewrite (16) as (17) where $y = \ln(A_0 h_l h_a/h)$ as Rician pointing error model case. After applying the integral identity of [15, eq. (3.462.1)], we can derive the composite PDF for Hoyt model as

$$\begin{aligned} f(h) =& \frac{\varepsilon_x \varepsilon_y h^{\frac{\varepsilon_x^2+\varepsilon_y^2}{2}-1}}{(A_0 h_l)^{\frac{\varepsilon_x^2+\varepsilon_y^2}{2}}\sqrt{2\pi}} \\ & \times \exp\left(-\frac{A^2(h)}{4}+2\sigma_X^2\frac{\varepsilon_x^2+\varepsilon_y^2}{2}+2\sigma_X^2\left(\frac{\varepsilon_x^2+\varepsilon_y^2}{2}\right)^2\right) \\ & \times \sum_{k=0}^{\infty}\frac{\Gamma(2k+1)}{(k!)^2}\left(\frac{\sigma_X\left(\varepsilon_y^2-\varepsilon_x^2\right)}{2}\right)^{2k} D_{-2k-1}(A(h)). \end{aligned} \tag{18}$$

A.3 Nonzero Mean Single-sided Gaussian

Along the same line, the composite PDF for nonzero mean single-sided case can be obtained by substituting (7) and (2) into (11) as

$$\begin{aligned} f(h) =& \frac{\varepsilon h^{\varepsilon^2-1} e^{-\frac{\mu^2}{2\sigma^2}}\sqrt{\mu}}{2^{\frac{3}{4}}(A_0 h_l)^{\varepsilon^2}\sqrt{2\pi\sigma_X^2 w_{z_{eq}}}} \\ & \times \int_{\frac{h}{A_0 h_l}}^{\infty} \frac{h_a^{-\varepsilon^2-1}}{\left(\ln\frac{A_0 h_l h_a}{h}\right)^{\frac{1}{4}}} I_{-\frac{1}{2}}\left(\frac{2\mu\varepsilon^2}{w_{z_{eq}}}\sqrt{2\ln\frac{A_0 h_l h_a}{h}}\right) \\ & \times \exp\left(-\frac{\left(\ln h_a + 2\sigma_X^2\right)^2}{8\sigma_X^2}\right) dh_a. \end{aligned} \tag{19}$$

After the similar mathematical procedure and manipulation, (19) can be expressed as (20) which includes an integral form that the integral identity of [15, eq. (3.462.1)] can be applied to solve. Finally, we can obtain the composite PDF as

$$\begin{aligned} f(h) =& \frac{\varepsilon e^{-\frac{\mu^2}{2\sigma^2}} h^{\varepsilon^2-1}}{2(A_0 h_l)^{\varepsilon^2}\sqrt{\pi\sigma_X}} \\ & \times \exp\left(-\frac{A^2(h)}{4}+2\sigma_X^2\varepsilon^2+2\sigma_X^2\varepsilon^4\right) \\ & \times \sum_{k=0}^{\infty}\frac{1}{k!}\left(\frac{\mu^2 w^2 \sigma_X}{4\sigma^4}\right)^k D_{-k-\frac{1}{2}}(A(h)). \end{aligned} \tag{21}$$

B. Unified Expression

Similarity of (15), (18), and (21) allows us to unify as

$$\begin{aligned} f(h) =& \nu(\varepsilon_x, \varepsilon_y, s, \rho_x, \rho_y) h^{\frac{\varepsilon_x^2+\varepsilon_y^2}{2}-1} \\ & \times e^{-\frac{A^2(h)}{4}} \sum_{k=0}^{\infty} B(k) D_{\alpha(k)}(A(h)), \end{aligned} \tag{22}$$

Table 3. Functions for unified expression.

Pointing error model	$B(k)$
Rician	$\frac{1}{k!}\left(\frac{s^2 w_{z_{eq}}^2 \sigma_X}{4\sqrt{2}\sigma^4}\right)^k$
Hoyt	$\frac{\Gamma(2k+1)}{(k!)^2}\left(\frac{\sigma_X\left(\varepsilon_y^2-\varepsilon_x^2\right)}{2\sqrt{2}}\right)^{2k}$
Nonzero mean single sided	$\frac{1}{\sqrt{\sqrt{2}\sigma_X}}\frac{1}{k!}\left(\frac{\mu^2 w_{z_{eq}}^2 \sigma_X}{4\sqrt{2}\sigma^4}\right)^k$

Table 4. Parameters for unified expression.

Pointing error	ε_x	ε_y	s	ρ_x	ρ_y	$\alpha(k)$
Rician	ε	ε	s	1	1	$-k-1$
Hoyt	ε_x	ε_y	0	1	1	$-2k-1$
Nonzero mean single	ε	0	μ	1	0	$-k-\frac{1}{2}$

where

$$\begin{aligned} & \nu(\varepsilon_x, \varepsilon_y, s, \rho_x, \rho_y) \\ & = \frac{\exp\left(-\frac{s^2}{2\sigma^2}+2\sigma_X^2\left(\frac{\varepsilon_x^2+\varepsilon_y^2}{2}\right)+2\sigma_X^2\left(\frac{\varepsilon_x^2+\varepsilon_y^2}{2}\right)^2\right)}{(A_0 h_l)^{\frac{\varepsilon_x^2+\varepsilon_y^2}{2}}\sqrt{2\pi}(\varepsilon_x+1-\rho_x)^{-\rho_x}(\varepsilon_y+1-\rho_y)^{-\rho_y}}. \end{aligned} \tag{23}$$

In Table 3, we specialize the unified PDF results given in (22) through functions of $B(k)$ for each of the pointing error models where constants are listed in Table 4.

IV. PERFORMANCE ANALYSIS

BER for a given signal-to-noise ratio (SNR) is [17]

$$\mathrm{BER}(\gamma) = \frac{\Gamma(p, q\gamma)}{2\Gamma(p)}, \tag{24}$$

where p defines detection mechanism (i.e., $p = 1$ for IM/DD and $p = \frac{1}{2}$ for HD), while q denotes index for modulation type (i.e., $q = 1$ for PSK and $q = \frac{1}{2}$ for FSK).

A. IM/DD

For IM/DD technique, instantaneous electrical SNR is defined as $\gamma = \left(\eta_e^2 h^2/N_0\right)$ [11]. Then, the average electrical SNR can be written as $\mu_{IM/DD} = \left(\eta_e^2 \mathbb{E}_h^2[h]/N_0\right)$. Since h_a and h_p are statistically independent processes, and h_l is deterministic, we can express the average electrical SNR as

$$\mu_{IM/DD} = \frac{\eta_e^2 h_l^2 \mathbb{E}_{h_p}^2[h_p]\,\mathbb{E}_{h_a}^2[h_a]}{N_0}. \tag{25}$$

Substituting (3) with $n = 1$ and first moment of h_p with $\varepsilon^2 \gg 1$ for each pointing error model into (25), we obtain

$$\mu_{IM/DD} = \frac{\eta_e^2 A_0^2 h_l^2 c^2 e^{4\sigma_X^2}}{N_0}, \tag{26}$$

$$f(h)=\frac{\varepsilon_x\varepsilon_y h^{\frac{\varepsilon_x^2+\varepsilon_y^2}{2}-1}}{2(A_0h_l)^{\frac{\varepsilon_x^2+\varepsilon_y^2}{2}}\sqrt{2\pi\sigma_X^2}}\left(\frac{h}{A_0h_l}\right)^{-\frac{\varepsilon_x^2+\varepsilon_y^2}{2}-\frac{1}{2}}\exp\left(-\frac{\left(\ln\frac{h}{A_0h_l}\right)^2}{8\sigma_X^2}-\frac{\sigma_X^2}{2}\right)\sum_{k=0}^{\infty}\frac{1}{(k!)^2}\left(\frac{\varepsilon_x^2-\varepsilon_y^2}{4}\right)^{2k}\times\int_0^{\infty}y^{2k}\exp\left(-\frac{y^2}{8\sigma_X^2}-\left(\frac{\ln\frac{h}{A_0h_l}}{4\sigma_X^2}+\frac{\varepsilon_x^2+\varepsilon_y^2}{2}+\frac{1}{2}\right)y\right)dy \tag{17}$$

$$f(h)=\frac{\varepsilon h^{\varepsilon^2-1}e^{-\frac{\mu^2}{2\sigma^2}}\sqrt{\mu}}{2^{\frac{3}{4}}(A_0h_l)^{\varepsilon^2}\sqrt{2\pi\sigma_X^2w_{z_{eq}}}}\left(\frac{h}{A_0h_l}\right)^{-\varepsilon^2-\frac{1}{2}}\exp\left(-\frac{\left(\ln\frac{h}{A_0h_l}\right)^2}{8\sigma_X^2}-\frac{\sigma_X^2}{2}\right)\sum_{k=0}^{\infty}\frac{\left(\frac{\sqrt{2}\mu\varepsilon^2}{w_{z_{eq}}}\right)^{2k-\frac{1}{2}}}{k!\Gamma\left(k+\frac{1}{2}\right)}\times\int_0^{\infty}y^{k-\frac{1}{2}}\exp\left(-\frac{y^2}{8\sigma_X^2}-\left(\frac{\ln\frac{h}{A_0h_l}}{4\sigma_X^2}+\varepsilon^2+\frac{1}{2}\right)y\right)dy \tag{20}$$

where c can be given as, respectively

$$\begin{aligned}c_{\text{Rician}}&=\exp\left(-\frac{2s^2}{w_{z_{eq}}^2}\right),\\ c_{\text{Hoyt}}&=1,\\ c_{\text{nonzero-single}}&=\exp\left(-\frac{2\mu^2}{w_{z_{eq}}^2}\right).\end{aligned} \tag{27}$$

The SNR γ, can be written in respect to $\mu_{IM/DD}$ as

$$\gamma=\frac{\mu_{IM/DD}}{(A_0h_lc)^2}h^2. \tag{28}$$

By utilizing (24) with (28), and PDF of γ, $f_\gamma(\gamma)$, the average BER in case of IM/DD can be obtained as

$$P_{e,IM,DD}=\int_0^{\infty}\frac{\Gamma\left(1,q\frac{\mu_{IM/DD}}{(A_0h_lc)^2}h^2\right)}{2\Gamma(1)}f(h)\,dh. \tag{29}$$

With [16, eq. (06.06.03.0008.01)], we can transform the gamma function in (29) into exponential function and by substituting (22), (29) can be written as

$$P_{e,IM,DD}=\int_0^{\infty}\frac{\exp\left(-q\frac{\mu_{IM/DD}}{(A_0h_lc)^2}h^2\right)}{2}\nu(\varepsilon_x,\varepsilon_y,s,\rho_x,\rho_y)\times h^{\frac{{\varepsilon_x}^2+{\varepsilon_y}^2}{2}-1}e^{-\frac{A^2(h)}{4}}\sum_{k=0}^{\infty}B(k)D_{\alpha(k)}(A(h))\,dh. \tag{30}$$

Using Taylor series expansion of exponential function and swapping the integration and summation with mathematical manipulation, we can express (30) as

$$P_{e,IM/DD}=\frac{1}{2}\sum_{n=0}^{\infty}\sum_{k=0}^{\infty}\frac{\left(-q\frac{\mu_{IM/DD}}{(A_0h_lc)^2}\right)^nB(k)P(\alpha(k),2n)}{n!\nu^{-1}(\varepsilon_x,\varepsilon_y,s,\rho_x,\rho_y)}, \tag{31}$$

where

$$P(\alpha(k),\beta(n))=\int_0^{\infty}h^{\beta(n)+\frac{{\varepsilon_x}^2+{\varepsilon_y}^2}{2}-1}e^{-\frac{A^2(h)}{4}}D_{\alpha(k)}(A(h))dh. \tag{32}$$

Applying change of variable, we can rewrite (32) as

$$P(\alpha(k),\beta(n))=2\sigma_X\left(A_0h_l\exp\left(-2\sigma_X^2-4\sigma_X^2\frac{\varepsilon_x^2+\varepsilon_y^2}{2}\right)\right)^{\frac{\varepsilon_x^2+\varepsilon_y^2}{2}+\beta(n)}\times\bar{P}(\alpha(k),\beta(n)), \tag{33}$$

where

$$\bar{P}(\alpha(k),\beta(n))=\int_{-\infty}^{\infty}\exp\left(-\frac{A^2}{4}+2\sigma_X\left(\frac{\varepsilon_x^2+\varepsilon_y^2}{2}+\beta(n)\right)A\right)D_{\alpha(k)}(A)\,dA. \tag{34}$$

Therefore, we can express the average BER as

$$P_{e,IM/DD}=\frac{1}{2}\sum_{n=0}^{\infty}\sum_{k=0}^{\infty}\frac{\left(-q\frac{\mu_{IM/DD}}{(A_0h_lc)^2}\right)^nB(k)\bar{P}(\alpha(k),2n)}{n!\bar{\nu}^{-1}(2n|\varepsilon_x,\varepsilon_y,s,\rho_x,\rho_y)}, \tag{35}$$

where

$$\bar{\nu}(\beta(n)|\varepsilon_x,\varepsilon_y,s,\rho_x,\rho_y)=\frac{\sqrt{2}\sigma_X(A_0h_l)^{\beta(n)}(\varepsilon_x+1-\rho_x)^{\rho_x}(\varepsilon_y+1-\rho_y)^{\rho_y}}{\sqrt{\pi}\exp\left(\frac{s^2}{2\sigma^2}+2\sigma_X^2\left(\frac{\varepsilon_x^2+\varepsilon_y^2}{2}\right)^2+\beta(n)\left(2\sigma_X^2+4\sigma_X^2\frac{\varepsilon_x^2+\varepsilon_y^2}{2}\right)\right)}. \tag{36}$$

The special function $\bar{P}(\alpha(k),\beta(n))$ can be obtained as follows. By partitioning the integration interval in (34) into $[-\infty,0]$ and $[0,\infty]$, we can rewrite (34) as

$$\bar{P}(\alpha(k),\beta(n))=\bar{P}_-(\alpha(k),\beta(n))+\bar{P}_+(\alpha(k),\beta(n)), \tag{37}$$

where $\bar{P}_-(\alpha(k),\beta(n))$ represents the $[-\infty,0]$ part and $\bar{P}_+(\alpha(k),\beta(n))$ represents the $[0,\infty]$ part. Using Taylor series, we transform $\exp\left(2\sigma_X\left(\frac{\varepsilon_x^2+\varepsilon_y^2}{2}+\beta(n)\right)A\right)$ in $\bar{P}_+(\alpha(k),\beta(n))$ into series form as

$$\bar{P}_+(\alpha(k),\beta(n))=\sum_{i=0}^{\infty}\frac{1}{i!}\left(2\sigma_X\left(\frac{\varepsilon_x^2+\varepsilon_y^2}{2}+\beta(n)\right)\right)^i\times\int_0^{\infty}e^{-\frac{A^2}{4}}A^iD_{-k-1}(A)\,dA. \tag{38}$$

With integral identity [16, eq. (07.41.21.0014.01)], $\bar{P}_{+}\left(\alpha\left(k\right),\beta\left(n\right)\right)$ can be derived as

$$\bar{P}_{+}\left(\alpha\left(k\right),\beta\left(n\right)\right)=\sum_{i=0}^{\infty}\frac{1}{i!}\left(2\sigma_X\left(\frac{\varepsilon_x^2+\varepsilon_y^2}{2}+\beta\left(n\right)\right)\right)^{i}\times\frac{\sqrt{\pi}\Gamma\left(i+1\right)}{2^{\frac{i+k+2}{2}}\Gamma\left(\frac{i+k+3}{2}\right)}\times{}_2F_1\left(\frac{i+1}{2},\frac{i+2}{2};\frac{i+k+3}{2};0\right). \tag{39}$$

Utilizing [16, eq. (07.41.26.0043.01)], $\bar{P}_{-}\left(\alpha\left(k\right),\beta\left(n\right)\right)$ can be expressed through Meijer G function [15, eq. (9.301)] as

$$\bar{P}_{-}\left(\alpha\left(k\right),\beta\left(n\right)\right)=2^{\frac{-k-1}{2}}\times\int_0^{\infty}\exp\left(-2\sigma_X\left(\frac{\varepsilon_x^2+\varepsilon_y^2}{2}+\beta\left(n\right)\right)A\right)\mathrm{G}_{2,3}^{2,1}\left(\frac{A^2}{2}\;\middle|\;\begin{matrix}\frac{-k+2}{2},\frac{-k}{2}\\0,\frac{1}{2},\frac{-k}{2}\end{matrix}\right)dA, \tag{40}$$

and with integral identity [15, eq. (7.813.2)], we can derive $\bar{P}_{-}\left(\alpha\left(k\right),\beta\left(n\right)\right)$ as

$$\bar{P}_{-}(\alpha(k),\beta(n))=\frac{\mathrm{G}_{4,3}^{2,3}\left(\frac{1}{2\sigma_X^2\left(\frac{\varepsilon_x^2+\varepsilon_y^2}{2}+\beta(n)\right)^2}\;\middle|\;\begin{matrix}0,\frac{1}{2},\frac{k+2}{2},\frac{-k}{2}\\0,\frac{1}{2},\frac{-k}{2}\end{matrix}\right)}{2^{\frac{k+3}{2}}\sqrt{\pi}\sigma_X\left(\frac{\varepsilon_x^2+\varepsilon_y^2}{2}+\beta\left(n\right)\right)}. \tag{41}$$

B. Heterodyne Detection

The instantaneous electrical SNR is given as $\gamma=\eta_e h/N_0$ [11]. Similarly, we can express the average electrical SNR as $\mu_{HD}=\left(\eta_e A_0 h_l c/N_0\right)$, where c is given as (27), and the instantaneous electrical SNR can be expressed in terms of μ_{HD} as

$$\gamma=\frac{\mu_{HD}}{A_0 h_l c}h. \tag{42}$$

With (24) and (42), we can derive average BER for HD as

$$P_{e,HD}=\int_0^{\infty}\frac{\Gamma\left(\frac{1}{2},q\frac{\mu_{HD}}{A_0h_lc}h\right)}{2\Gamma\left(\frac{1}{2}\right)}f\left(h\right)dh. \tag{43}$$

Applying series expansion of incomplete gamma function [16, eq. (06.06.06.0002.01)], (43) leads to

$$P_{e,HD}=\frac{1}{2\Gamma\left(\frac{1}{2}\right)}\times\left[\Gamma\left(\frac{1}{2}\right)\int_0^{\infty}f\left(h\right)dh-\sum_{n=0}^{\infty}\frac{(-1)^n\left(\frac{q\mu_{HD}}{A_0h_lc}\right)^{n+\frac{1}{2}}}{n!\left(n+\frac{1}{2}\right)}\int_0^{\infty}h^{n+\frac{1}{2}}f(h)dh\right]. \tag{44}$$

In a similar way as IM/DD case, (44) can also be expressed through $\bar{P}(\alpha\left(k\right),\beta\left(n\right))$ and $\bar{\nu}\left(\beta\left(n\right)|\varepsilon_x,\varepsilon_y,s,\rho_x,\rho_y\right)$ as

$$P_{e,HD}=\frac{\bar{\nu}\left(\varepsilon_x,\varepsilon_y,s,\rho_x,\rho_y\right)}{2\Gamma\left(\frac{1}{2}\right)}\left[\sum_{k=0}^{\infty}B\left(k\right)\Gamma\left(\frac{1}{2}\right)\bar{P}\left(\alpha\left(k\right),0\right)-\sum_{n=0}^{\infty}\frac{\left(\frac{q\mu_{HD}}{A_0h_lc}\right)^{n+\frac{1}{2}}B\left(k\right)}{(-1)^{-n}n!\left(n+\frac{1}{2}\right)}\bar{P}\left(\alpha\left(k\right),n+\frac{1}{2}\right)\right]. \tag{45}$$

V. NUMERICAL RESULTS

In this section, with exact Monte-Carlo simulations, our derived results of average BER (i.e., (35) and (45)) are cross-verified with simulation results. Using the parameter setting listed in Table 5, average BER curves are plotted against the average electrical SNR μ for IM/DD and HD in Figs. 2 and 3, respectively. Both Figs. 2and 3 considered the three pointing errors models (i.e., Rician, Hoyt and Nonzeromean) with parameter values in Table 6 and weak turbulence models with different Rytov variance value (i.e., $\sigma_R^2=0.05$ and $\sigma_R^2=0.2$).

First, as the analytical results and simulation results match each other, we confirm that expressions (35) and (45) provide a precise evaluation. Since greater value of Rytov variance leads to stronger turbulence, it can be easily found from Figs. 2 and 3 that the BER performance of $\sigma_R^2=0.2$ is worse than that of $\sigma_R^2=0.05$. From the parameter values in Table 6, the Rician model represents the worst pointing error model with boresight and jitter in two axes. Also, the Hoyt model describes the error caused by only jitter which gives constant movement with larger value in the y axis than x axis. Lastly for the non-zero mean model, the error occurs by only x axis with dominant value of boresight.

From Fig. 2, we find that the Rician model shows the worst error rate performance and the curve of Rician model with $\sigma_R^2=0.05$ shows worse performance than that of other pointing error models with $\sigma_R^2=0.2$. It can be confirmed that with the parameter values listed in Table 6, the effect of Rician pointing error is greater than that of turbulence with $\sigma_R^2=0.2$. Also, we note that as the SNR value increases up to a certain point, the BER curves of Hoyt model and the curves of non-zero mean model are reversed at that point. Therefore, we can infer that the effect of boresight is dominant compared to jitter in low SNR region, and as the SNR value increases, the effect of the jitter becomes dominant compared to that of boresight. In other words, the fixed displacement between transmitter and receiver has greater effect on BER performance in low SNR region, and the random offset has greater effect in high SNR region. Comparing Figs. 2 and 3, we can see the performance of IM/DD and that of HD are similarly affected by the pointing error and turbulence. However, it is obvious that HD shows greater error performance.

VI. CONCLUSION

In this paper, we pointed out the pointing error models that can occur in FSO communication between shore and ship or

Table 5. Parameter settings.

Parameter	Symbol	Value
Receiver radius	a	10 cm
Beamwidth	w_z	100 cm
Modulation type	q	1
Attenuation coefficient	σ	1.10622
Distance between Tx and Rx	z	1 km

Table 6. Pointing error settings.

Axis		Single-sided	Double-sided	
Error type		Nonzero mean	Rician	Hoyt
Boresight (cm)	μ_x	30	30	0
	μ_y	0	30	0
Jitter (cm)	σ_x	5	20	5
	σ_y	0	20	20

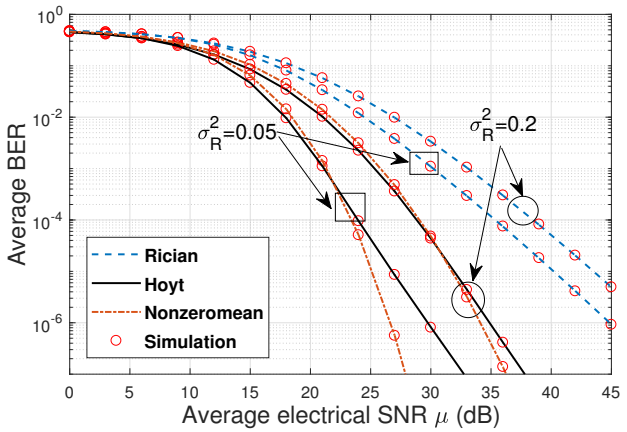

Fig. 2. Average BER of IM/DD FSO link under weak turbulence (i.e., $\sigma_R^2 = 0.05$ and $\sigma_R^2 = 0.2$) combined with pointing error models.

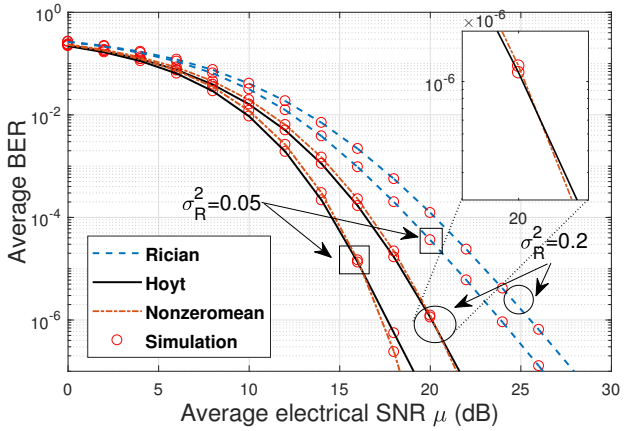

Fig. 3. Average BER of HD FSO link under weak turbulence (i.e., $\sigma_R^2 = 0.05$ and $\sigma_R^2 = 0.2$) combined with pointing error models.

ships. Based on the modeled results, we statistically derived the unified composite PDF containing all possible pointing error models based on weak turbulence model. In addition, we analyzed BER performance in FSO communication with IM/DD and HD technology based on the derived unified composite PDF results. Then, with exact Monte-Carlo simulations, our derived analytical results of average BER (i.e., (35) and (45)) were cross-verified with simulation results under various pointing error models and weak turbulence conditions. From some selected results, the effects of Rytov dispersion, aiming, and jitter on the BER performance were identified.

REFERENCES

[1] K. Jung, S. S. Nam, M. Alouini and, Y. Ko, "Unified statistical channel model of ship (or shore)-to-ship FSO communications with pointing errors," in *Proc. IEEE CSCN*, 2019.

[2] I. KeunSon, S. Mao, "A survey of free space optical networks," *Digit. Commun. Netw.*, vol. 3, no. 11, Nov.. 2016.

[3] Campbell,P.(2017,August 28). Research demonstrate high-bandwidth communications capability for ships. [Online]. Available: https://phys.org/news/2017-08-high-bandwidth-capability-ships.html

[4] F. Yang, J. Cheng, and T. Tsiftsis, "Free-space optical communication with nonzero boresight pointing errors," *IEEE Trans. Commun.*, vol. 62, no. 2, pp. 713–725, Feb. 2014.

[5] A. Farid and S. Hranilovic, "Outage capacity optimization for free-space optical links with pointing errors," *IEE/OSA J. Lightwave Technol.*, vol. 25, no. 7, pp. 1702–1710, July. 2007.

[6] I. S. Ansari, M. Alouini, and J. Cheng, "On the capacity of FSO links under lognormal and Rician-lognormal turbulences," in *Proc. IEEE VTC*, Sept. 2014.

[7] M. Yasser, T. Ismail, and A. Ghuniem, "M-ary ASK modulation in FSO system with SIMO over log-normal atmospheric turbulence with pointing errors," in *Proc. CSNDSP*, July 2018.

[8] T. Ismail and E. Leitgeb, "Performance analysis of SIM-DPSK FSO system over lognormal fading with pointing errors," in *Proc. ICTON*, July 2016.

[9] Y. Zhang, S. Tang, and J. Wang, "Average bit error rate performance of direct current biased orthogonal frequency division multiplexing in free-space optical communications over weak turbulence," in *Proc. WCSP*, Oct. 2014.

[10] G. K. Varotsos, H. E. Nistazakis, M. I. Petkovic, G. T. Djordjevic, and G. S. Tombras, "SIMO optical wireless links with nonzero boresight pointing errors over M modeled turbulence channels," *Optics Commun.*, vol. 403, pp. 391–400, Nov. 2017.

[11] H. Al-Quwaiee, H. C. Yang, and M. S. Alouini, "On the asymptotic ergodic capacity of FSO links with generalized pointing error model," in *Proc. IEEE ICC*, June 2015.

[12] K. Jung, S. S. Nam, M. Alouini, and Y. Ko, "Unified finite series approximation of FSO performance over strong turbulence combined with various pointing error conditions," King Abdullah University of Science and Technology (KAUST), Tech. Rep., 2020. [Online]. Available: http://hdl.handle.net/10754/661871

[13] M. Naboulsi, H. Sizun, and F. Fornel, "Propagation of optical and infrared waves in the atmosphere," in *Proc. URSI*, Oct. 2005.

[14] M. Al-Habash, L. C. Andrews, and R. L. Phillps, "Mathematical model for the irradiance probability density function of a laser beam propagating through turbulent media," *Opt Eng*, vol. 62, no. 2, pp. 1554–1562, Feb. 2001.

[15] I. S. Gradshteyn and I. M. Ryzhik, Table of Integrals, Series, and Products, 6th ed. New York: Academic, 2000.

[16] Wolfram, "The wolfram functions," [Online]. Available: http://functions.wolfram.com/

[17] A. H. Wojnar, "Unknown bounds on performance in Nakagami channels," *IEEE Trans. Commun.*, vol. 34, no. 1, pp. 22–24, Jan. 1986.

Kug-Jin Jung received the B.S. and M. S. degrees in Electrical Engineering from Korea University, Seoul, South Korea, in 2016 and 2018, respectively, where he is currently pursuing the Ph.D. degree with the School of Electrical Engineering. In 2019, he visited King Abdullah University of Science and Technology (KAUST), Thuwal, Saudi Arabia, to conduct a collaborative research. His current research interest includes free space optics, performance analysis of wireless communication system, and centralized radio access network.

Sung Sik Nam (S'05–M'09) received the B.S. and M.S. degrees in Electronic Engineering from Hanyang University, Korea, in 1998 and 2000, respectively. Also, he received the M.S. degree in Electrical Engineering from University of Southern California, USA, in 2003, and the Ph.D. degree at Texas A&M University, College Station, USA, in 2009. From 1998 to 1999, he worked as a researcher at ETRI, Korea. From 2003 through 2004, he worked as a manager at the Korea Telecom Corporation, Korea. From 2009 to 2010 and from 2011 to 2013, he was with Hanyang University and Sungkyunkwan University, Korea, respectively. From 2013 to 2016, he was with Hanyang University, Korea. From 2017 to 2019, he was with Korea University, Korea before joining Gachon University, Korea as an assistant professor of Department of Electronic Engineering in 2020. His research interests include the design and performance analysis of wireless communication system, diversity techniques, power control, multiuser scheduling, cooperative communications, energy harvesting, and wireless optical communication.

Jinwoo Shin received the B.S., M.S., and Ph.D. degrees in Electrical and Computer Engineering from the University of Seoul, Seoul, Korea, in 1995, 1997, and 2014, respectively. He has been with Agency for Defense Development, Daejeon, Korea, since 1997. His current research interests include the numerical modeling and analysis of wideband phase array system, radar and terahertz applications

Young-Chai Ko (S97-M01-SM06) received the B.Sc. degree in Electrical and Telecommunication Engineering from the Hanyang University, Seoul, Korea and the M.S.E.E. and Ph.D. degrees in Electrical Engineering from the University of Minnesota, Minneapolis, MN in 1999 and 2001, respectively. He was with Novatel Wireless as a Research Scientist from January 2001 to March 2001. In March 2001, he joined the Texas Instruments, Inc., wireless center, San Diego, CA, as a Senior Engineer. He is now with the School of Electrical Engineering at Korea University as a Professor. His current research interests include the design and evaluations of multiuser cellular system, MODEM architecture, mm-wave and Tera Hz wireless systems.